Appl. Phys. B (2013) 113:165–170
DOI 10.1007/s00340-013-5710-0

Applied Physics B
Lasers and Optics

RAPID COMMUNICATION

# Controllable vector bottle-shaped fields generated by focused spatial-variant linearly polarized vector beams

**Bing Gu · Jia-Lu Wu · Yang Pan · Yiping Cui**

Received: 26 August 2013 / Accepted: 21 October 2013 / Published online: 2 November 2013


**Abstract** We demonstrate that the optical bottle-shaped fields can be controllably generated by the focused spatial-variant linearly polarized vector beams. Based on the vectorial Rayleigh–Sommerfeld formulas under the paraxial approximation, we present theoretically the analytical expression for the focused field of the vector beam and predict the evolution of the sate of polarization (SoP) in the focal region. Experimentally, we observe the vector bottle-shaped field that is in agreement with the numerical simulations. In particular, we validate that both the SoP and the size of the optical bottle field are manipulated easily by varying the azimuthal topological charge and the radial mode index.

## 1 Introduction

In the past few years, the optical bottle-shaped field, which consists of low intensity surrounded by regions of higher intensity, has received extensively attention due to its specific applications in optical tweezers for trapping and manipulating different micro-objects, including light-absorbing particles [1–4], cold atoms [5–7], and particles with a refractive index lower than that of the surrounding medium [8]. Up to now, the optical bottle field has been generated by many methods. For examples, Arlt and Padgett [9] obtained the optical bottle beam arising from destructive interference between two linearly polarized Laguerre-Gaussian modes with different Gouy phases. Shvedov et al. [10] generated linearly polarized optical bottle beams by double-charge white-light optical vortices. Chremmos et al. [11] demonstrated elegant paraboloid optical bottles formed by Fourier-transforming lens. Alpmann et al. [3] reported the generation of holographic optical bottle beams to manipulate absorbing particles. Genevet et al. [12] presented two-dimensional plasmonic bottle beams by the interference of a non\diffracting beam. It is noteworthy that all these methods are concentrated on shaping the intensity distribution while ignoring the polarization distribution of light.

As an intrinsic vectorial nature of light, polarization plays an important role in the interaction of light with matter. Very recently, researchers used cylindrical vector beams to trap micrometer-sized dielectric particles [13], gold nanoparticles [14], and carbon nanotubes [15]. It is well established that the trapping efficiency depends strongly on the intensity profile and the SoP of the trapping beam [13–15]. Besides, Skelton et al. [16] have demonstrated that the polarization dependence adds additional flexibility to control the optical trap strength in optical tweezers. Therefore, it is highly desirable to generate the controllable bottle-shaped field with the desired polarization distribution for contactless manipulation of micro-objects. However, reports of vector bottle-shaped beams are sporadic in the literature. As an example, Shvedov et al. [17] have generated vector bottle beams with a uniaxial crystal very recently.

In this work, we report a theoretical and experimental investigation of the focused spatial-variant linearly polarized vector beams. By varying the azimuthal topological

B. Gu (✉) · J.-L. Wu · Y. Pan · Y. Cui
Advanced Photonics Center, Southeast University, Nanjing 210096, China
e-mail: gubing@seu.edu.cn

Y. Cui
e-mail: cyp@seu.edu.cn

B. Gu
Jiangsu Key Laboratory on Opto-Electronic Technology, Nanjing Normal University, Nanjing 210046, China

charge and the radial mode index of the vector beam, we demonstrate that both the SoP and the size of the vector bottle-shaped field can be easily manipulated.

## 2 Theory

The electric field distribution of the spatial-variant linearly polarized vector beam at the $z = 0$ plane can be expressed as [18]

$$\mathbf{E}(r,\phi,0) = E_r(r,\phi,0)\mathbf{e_r} + E_\phi(r,\phi,0)\mathbf{e_\phi}, \tag{1}$$

where

$$E_r(r,\phi,0) = A(r)\cos\left(\frac{2n\pi r^2}{r_0^2} + m\phi - \phi + \varphi_0\right), \tag{2}$$

$$E_\phi(r,\phi,0) = A(r)\sin\left(\frac{2n\pi r^2}{r_0^2} + m\phi - \phi + \varphi_0\right). \tag{3}$$

Here, $\mathbf{e_r}$ and $\mathbf{e_\phi}$ are the unit vectors in the polar coordinate system ($r$, $\phi$). The real number $n$ is the radial mode index, whereas the integer $m$ is the azimuthal topological charge, which can be positive or negative depending on the handedness of the orbital angular momentum. $\varphi_0$ and $r_0$ are the initial phase and the radius of the vector beam, respectively. $A(r)$ represents the radial-dependent amplitude. For the uniform-intensity beam focused by a thin lens with a focal length of $f$, we have $A(r) = E_0 \exp(-i k r^2/2f)$ for $0 \le r \le r_0$, else $A(r) = 0$. Here, $k = 2\pi/\lambda$ is the wavenumber and $\lambda$ is the wavelength of the laser. It should be emphasized that the spatial-variant linearly polarized vector beam has the spatial distribution of SoP with the simultaneous azimuthal and radial variant.

Based on the vectorial Rayleigh–Sommerfeld formulas under the paraxial approximation, the radial and azimuthal components of the electric field vector can be given by [19]

$$\begin{aligned} E_r(\rho,\theta,z) = -\frac{ik}{2\pi z}e^{ikz}\int_0^\infty\int_0^{2\pi}&[E_r(r,\phi+\theta,0)\cos\phi \\ &- E_\phi(r,\phi+\theta,0)\sin\phi] \\ &\times\exp\left(\frac{ikr^2}{2z}\right)\exp\left(-i\frac{k\rho}{z}r\cos\phi\right)r\mathrm{d}r\mathrm{d}\phi, \end{aligned} \tag{4}$$

$$\begin{aligned} E_\phi(\rho,\theta,z) = -\frac{ik}{2\pi z}e^{ikz}\int_0^\infty\int_0^{2\pi}&[E_r(r,\phi+\theta,0)\sin\phi \\ &+ E_\phi(r,\phi+\theta,0)\cos\phi] \\ &\times\exp\left(\frac{ikr^2}{2z}\right)\exp\left(-i\frac{k\rho}{z}r\cos\phi\right)r\mathrm{d}r\mathrm{d}\phi. \end{aligned} \tag{5}$$

It is noteworthy that the coordinate origin $z = 0$ is at the plane of the lens. Accordingly, one gets $z = f$ at the lens geometrical focus.

Substituting Eqs. (2) and (3) into Eqs. (4) and (5), and using the integral theorems [see Eq. (4) in [20] ] , we obtain

$$E_r(\rho,\theta,z) = \frac{(-i)^{m+1}kE_0}{2z}\exp(ikz)[A_1\exp(i\Psi) + A_2\exp(-i\Psi)], \tag{6}$$

$$E_\phi(\rho,\theta,z) = \frac{(-i)^{m+2}kE_0}{2z}\exp(ikz)[A_1\exp(i\Psi) - A_2\exp(-i\Psi)], \tag{7}$$

where

$$A_j(\rho,z) = \int_0^{r_0}\exp(-i\delta_j r^2)J_m(\beta r)r\mathrm{d}r, \quad (\mathrm{j} = 1,2). \tag{8}$$

Here, $\Psi = m\theta - \theta + \varphi_0$, $\delta_1 = k/(2f) - k/(2z) - 2n\pi/r_0^2$, $\delta_2 = k/(2f) - k/(2z) + 2n\pi/r_0^2$, and $\beta = k\rho/z$. $J_m(\cdot)$ is the Bessel function of $m$th order. Expanding the Bessel function into series and recalling the incomplete gamma function $\Gamma(\alpha,x) = \int_x^\infty e^{-t}t^{\alpha-1}\mathrm{d}t$ and the gamma function $\Gamma(\alpha) = \int_0^\infty e^{-t}t^{\alpha-1}dt$, we rewrite Eq. (8) as

$$\begin{aligned} A_j = &\sum_{l=0}^{\infty}\frac{(-1)^l\beta^{m+2l}}{2^{m+2l+1}l!(m+l)!(i\delta_j)^{m/2+l+1}} \\ &\times\left[\Gamma\left(\frac{m}{2}+l+1\right) - \Gamma\left(\frac{m}{2}+l+1, i\delta_j r_0^2\right)\right]. \end{aligned} \tag{9}$$

Equations (6) and (7) combined with Eq. (9) are the basic results of the present work, which provides an analytical expression for the electric components of a spatial-variant linearly polarized vector beam in the focal region under the paraxial approximation. Interestingly, the paraxial result can be regarded as a special case of the nonparaxial result. In the nonparaxial condition, the longitudinal component of electric field should be considered in the analysis. Similar to the focal field we presented in this work, the three-dimensional electric field can be derived by means of the vectorial Rayleigh–Sommerfeld formulas under the nonparaxial approximation [19].

The evolution of SoP of the focused spatial-variant linearly polarized vector beam is explored as follows. With the aid of $\mathbf{e_r} = (e^{-i\theta}\sigma_+ + e^{i\theta}\sigma_-)/\sqrt{2}$ and $\mathbf{e_\phi} = -i(e^{-i\theta}\sigma_+ - e^{i\theta}\sigma_-)/\sqrt{2}$, where $\sigma_+$ and $\sigma_-$ are the unit vectors of the left-handed (LH) and right-handed (RH) circular polarizations, respectively. Accordingly, we revise Eqs. (6) and (7) as

$$\mathbf{E}(\rho,\theta,z) = \frac{\sqrt{2}(-i)^{m+1}kE_0}{z}e^{ikz}[E_+\sigma_+ + E_-\sigma_-] \tag{10}$$

with $E_+ = A_1 \exp(im\theta + i\varphi_0)$ and $E_- = A_2 \exp(-im\theta - i\varphi_0)$. In general, the LH and RH circularly polarized components have different amounts (i.e., $|E_+|^2 \neq |E_-|^2$) due to $|A_1| \neq |A_2|$. Accordingly, the focused spatial-variant linearly polarized vector beams exhibit the hybrid SoP mainly originating from the localized elliptical polarization. And that the polarization evolution of a spatial-variant linearly polarized vector beam through the focus is observable, as we demonstrate in Fig. 5. Specially, for $z = f$ one gets $|A_1| = |A_2|$ (subsequently, $|E_+|^2 = |E_-|^2$) from Eq. (9), which suggests the focused spatial-variant linearly polarized vector beam with localized linear polarization at the lens' geometrical focal plane. If $n = 0$, one finds $A_1 = A_2$ for any values of both $z$ and $\rho$ from Eq. (9). In this case, the focused field preserves the localized linear polarization at any propagation position.

## 3 Experiment

The spatial-variant linearly polarized vector beams have been generated by many methods [21–24]. Following the same method presented by Wang et al. [18, 22] and using a 532-nm CW laser beam, we generate the spatial-variant linearly polarized vector beams with different values of $m$ and $n$ by a common path interferometer implemented with a computer-controlled spatial light modulator. The experimental arrangement and the detailed description can be found elsewhere [18, 22].

For the sake of simplicity, we only consider the vector beam for $\varphi_0 = 0$ in the whole analysis. Figure 1 illustrates the measured (top row) and simulated (lower row) intensity patterns of the vector beams with a horizontal polarizer. In fact, all the intensity patterns without the polarizer exhibiting the vector singularity at the center of the vector beam have no obviously different. Interestingly, the intensity patterns behind a polarizer exhibit the spiral structure. Furthermore, the number of arms is equal to $2m$ while is independent of $n$. Apparently, the spatial-variant linearly polarized vector beams have the rich SoP (see arrows in Fig. 1), compared with the azimuthal- or radial-variant vector beams [18, 22, 25]. The radius of all the generated vector beams is measured to be $r_0 = (1.90 \pm 0.05)$ mm.

To illustrate the propagation behaviors of the focused spatial-variant linearly polarized vector beams, numerical simulations have been performed using Eqs. (6) and (7) by taking $r_0 = 1.9$ mm, $\lambda = 532$ nm, and $f = 150$ mm. Figure 2 shows the intensity distributions of a vector beam with $m = 1$ and $n = 1$ in the focal region of the lens. Figure 2a displays the simulated intensity patterns through the lens' geometrical focus in the *XZ plane* ($y = 0$). It can be seen that the focused vector beam forms an optical bottle-shaped field with zero on-axis intensity surrounded by a cylindrical light wall. Figures 2b, c show the simulated and measured transverse intensity patterns taken at *planes* (1–5) with $\delta = 6.5$ mm marked in Fig. 1a, respectively. Obviously, the experimental results are in good agreement with the numerical simulations. It should be pointed out that the bottleneck of the generated bottle-shaped field is two bright rings, in contrast to that of bright spots [17, 26] or completely closed ends [11].

Numerical simulations indicate that (1) the diameter of the bottleneck $\Delta d$ increases as the value of $m$ increases while is independent of $n$, (2) the length of the optical bottle $\Delta z$ (namely the interval between two bottlenecks) is linearly increasing function of $n$ while is independent of $m$, and (3) the width of the optical bottle $\Delta D$ (i.e., the width of a vector beam at the lens' geometrical focus) increases as the values of $m$ and $n$ increase. This phenomenon can be understood as follows. It is well documented that the azimuthal-variant vector beam could be focused into the flower-like patterns [20, 27]. Numerical simulation indicates that the focused radial-variant vector beam exhibits bi-foci alone the optical axis. The focal volume of a spatial-variant linearly polarized vector beam is modulated by the azimuthal- and radial-variant SoP simultaneously. As a result, the width of the optical bottleneck is manipulated by the azimuthal topological charge whereas the length of the optical bottle is controlled by the radial mode index.

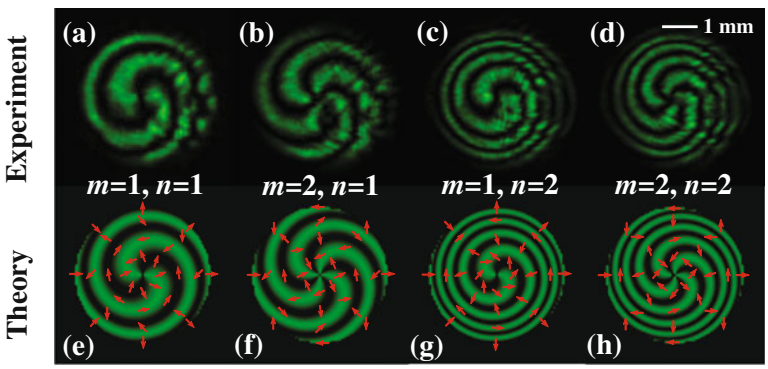


**Fig. 1** Measured (*top row*) and simulated (*lower row*) intensity patterns of the spatial-variant linearly polarized vector beams with a horizontal polarizer. The corresponding *arrows* in the *lower row* illustrate the schematics of SoP. The radii of all vector beams are $r_0 = 1.90$ mm

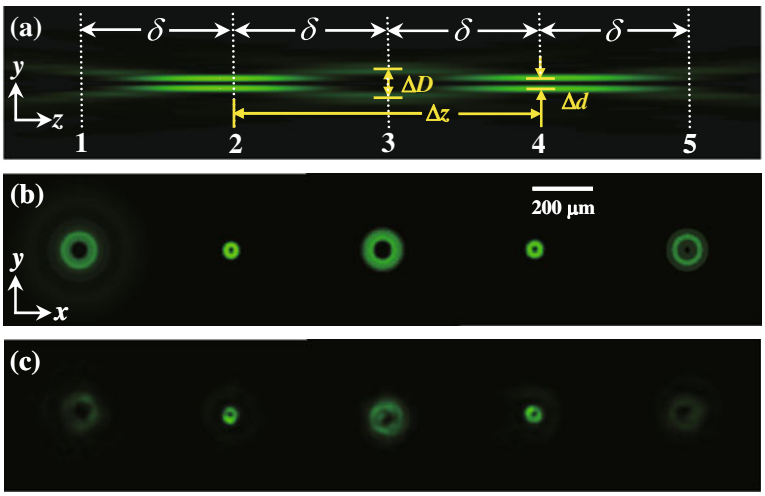


**Fig. 2** The optical bottle-shaped field generated by the focused spatial-variant linearly polarized vector beam with $m = 1$ and $n = 1$ when $r_0 = 1.9$ mm, $\lambda = 532$ nm, and $f = 150$ mm. **a** Simulated longitudinal intensity pattern of the focused vector beam in the *XZ plane*. Simulated **b** and measured **c** transverse intensity patterns taken at *planes* (1–5) with $\delta = 6.5$ mm marked in **a**. $\Delta d$ the diameter of the bottleneck; $\Delta D$ and $\Delta z$ the width and length of the optical bottle, respectively

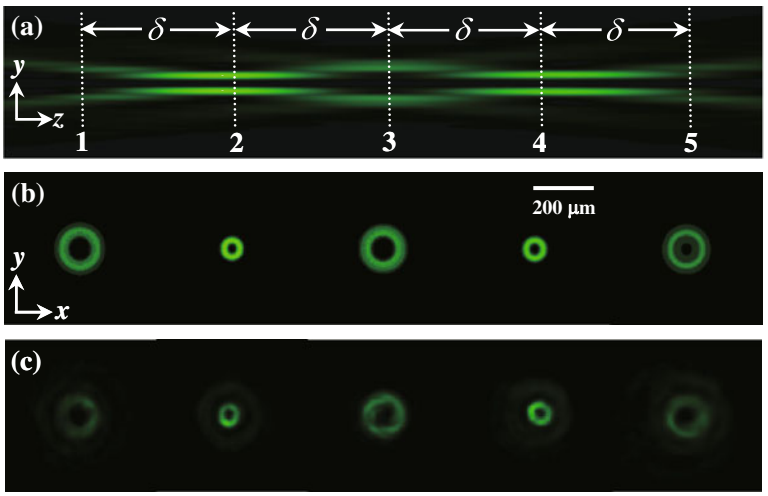


**Fig. 3** The optical bottle-shaped field generated by the focused spatial-variant linearly polarized vector beam with $m = 2$ and $n = 1$ when $r_0 = 1.9$ mm, $\lambda = 532$ nm, and $f = 150$ mm. **a** Simulated longitudinal intensity pattern of the focused vector beam in the *XZ plane*. Simulated **b** and measured **c** transverse intensity patterns taken at *planes* (*1–5*) with $\delta = 6.5$ mm marked in **a**

To verify our theoretical predictions, as examples, we measure the intensity distributions of the focused vector beams with $m = 2$ and $n = 1$ (see Fig. 3), and $m = 1$ and $n = 2$ (see Fig. 4). As can be seen from Figs. 2, 3, 4, the radius of the bottleneck increases as $m$ increase, while the length of the optical bottle increases with increasing the value of $n$. Specifically, the geometric sizes of the focused vector beams are summarized in Table 1. As shown in Table 1, both the width and length of the optical bottle are manipulated easily by tuning the azimuthal topological charge and the radial mode index of the generated vector beam.

Different from the conventional bottle-shaped field with homogeneously SoP [9, 11], the bottle-shaped field presented in this work has the inhomogeneous distribution of SoP. Figure 5 illustrates the optical bottle-shaped field generated by the focused vector beam with $m = 2$ and $n = 2$. To identify the vector behavior of the bottle field, a horizontal polarizer is used. Accordingly, the simulated and measured transverse intensity patterns with a horizontal polarizer at planes (1–5) marked in Fig. 5a are displayed in Figs. 5b, c, respectively. Clearly, the measured results are in consistent with the numerical simulations. Figure 5d shows the simulated transverse intensity patterns without a polarizer. As shown in Figs. 5b, c, the intensity patterns with a horizontal polarizer exhibit the spiral structure except for the symmetrical rings at planes of two bottlenecks. At planes of two bottlenecks, the focusing degree is stronger than that at any other plane. Accordingly, the difference between the LH and RH circularly polarized components is larger as described by Eq. (10), which indicates that the ellipticity $e$ of the localized elliptical polarization at the bottleneck is larger than that at any other plane, in contrast to $e = 0$ at the lens geometrical focal plane. Interestingly, the chiralities of the intensity patterns at both sides of the bottleneck are opposite. This is because the spatial-variant linearly polarized vector beam forms bi-focusing alone the optical axis. Thus, the direction of the optical field on both sides of the true focal plane is opposite. Most importantly, the

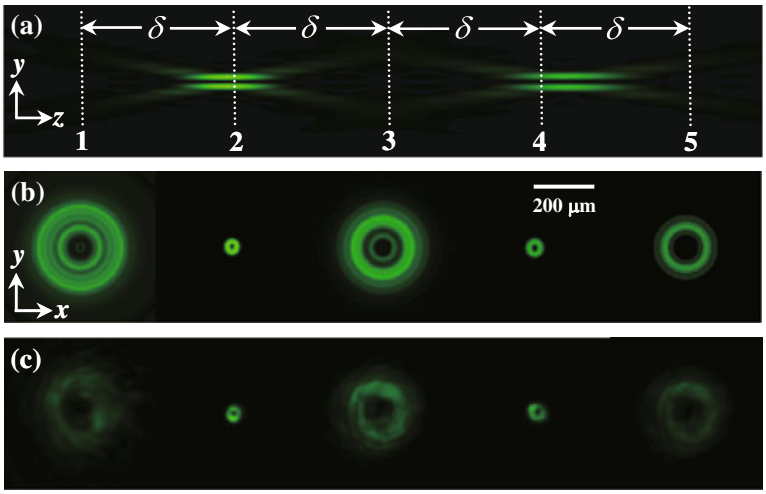


**Fig. 4** The optical bottle-shaped field generated by the focused spatial-variant linearly polarized vector beam with $m = 1$ and $n = 2$ when $r_0 = 1.9$ mm, $\lambda = 532$ nm, and $f = 150$ mm. **a** Simulated longitudinal intensity pattern of the focused vector beam in the *XZ plane*. Simulated **b** and measured **c** transverse intensity patterns taken at *planes* (*1–5*) with $\delta = 13$ mm marked in **a**

**Table 1** The geometric sizes of the optical bottle-shaped fields when $r_0 = 1.9$ mm, $\lambda = 532$ nm, and $f = 150$ mm

| Vector beam | $\Delta z$ (mm) | $\Delta D$ (um) | $\Delta d$ (um) |
|---|---|---|---|
| $m = 1, n = 1$ | 13 | 126 | 35 |
| $m = 2, n = 1$ | 13 | 141 | 62 |
| $m = 1, n = 2$ | 26 | 252 | 35 |

optical bottle-shaped field with hybrid SoP exhibits the complicated evolution of SoP at different positions, as shown in Fig. 5d. Specially, the optical bottle at the lens' geometrical focus is a localized linearly polarized field, as we predict in Sect. 2. The size of the bottle-shaped field is tunable by varying the topological charges of the vector beam. Analogously, the polarization distribution of the generated bottle field could be manipulated by tuning the azimuthal topological charge and the radial mode index. This vectorial behavior of the generated bottle field offers additional flexibility to control the optical trap strength in optical tweezers [16].

## 4 Conclusion

In summary, we have demonstrated, both theoretically and experimentally, that the vector bottle-shaped fields can be controllably generated by focused spatial-variant linearly polarized vector beams. Based on the vectorial Rayleigh–Sommerfeld formulas under the paraxial approximation, we have presented the analytical expression for the focused

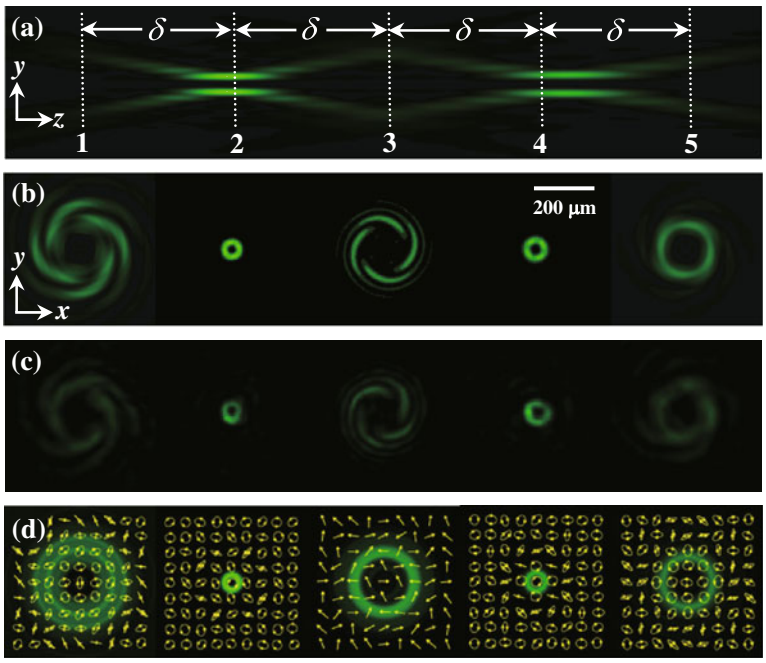


**Fig. 5** The optical bottle-shaped field generated by the focused spatial-variant linearly polarized vector beam with $m = 2$ and $n = 2$ when $r_0 = 1.9$ mm, $\lambda = 532$ nm, and $f = 150$ mm. **a** Simulated longitudinal intensity pattern of the focused vector beam in the *XZ plane*. Simulated **b** and measured **c** transverse intensity patterns with a horizontal polarizer taken at *planes* (*1–5*) with $\delta = 13$ mm marked in **a**. **d** Simulated transverse intensity patterns without a polarizer and the distribution of SoP at *planes* marked in **a**

field of the vector beam. Especially, we have found the polarization evolution of the focused spatial-variant linearly polarized vector beam. Experimentally, we have measured the bottle-shaped field with hybrid SoP, which is in agreement with the numerical simulations. Most importantly, we have demonstrated that both the SoP and the size of the optical bottle field are manipulated easily by varying the azimuthal topological charge and the radial mode index. This vectorial bottle field with controllable intensity profile and polarization distribution has prominent applications in optical tweezers for contactless trapping and manipulating micro-particles.

**Acknowledgements** This work was supported by the National Science Foundation of China (Grants: 11174160 and 10947004), Jiangsu Key Laboratory for Optoelectronics (Grant: 1640703061-9), and the Program for New Century Excellent Talents in University (Grant: NCET-10-0503).

## References

1. V.G. Shvedov, C. Hnatovsky, A.V. Rode, W. Krolikowski, Robust trapping and manipulation of airborne particles with a bottle beam. Opt. Express **19**, 17350–17356 (2011)
2. P. Zhang, Z. Zhang, J. Prakash, S. Huang, D. Hernandez, M. Salazar, D.N. Christodoulides, Z. Chen, Trapping and transporting aerosols with a single optical bottle beam generated by moiré techniques. Opt. Lett. **36**, 1491–1493 (2011)
3. C. Alpmann, M. Esseling, P. Rose, C. Denz, Holographic optical bottle beams. Appl. Phys. Lett. **100**, 111101 (2012)
4. Z. Zhang, P. Zhang, M. Mills, Z. Chen, D.N. Christodoulides, J. Liu, Trapping aerosols with optical bottle arrays generated through a superposition of multiple Airy beams. Chin. Opt. Lett. **11**, 033502 (2013)
5. T. Kuga, Y. Torii, N. Shiokawa, T. Hirano, Y. Shimizu, H. Sasada, Novel optical trap of atoms with a doughnut beam. Phys. Rev. Lett. **78**, 4713–4716 (1997)
6. L. Isenhower, W. Williams, A. Dally, M. Saffman, Atom trapping in an interferometrically generated bottle beam trap. Opt. Lett. **34**, 1159–1161 (2009)
7. P. Xu, X. He, J. Wang, M. Zhan, Trapping a single atom in a blue detuned optical bottle beam trap. Opt. Lett. **35**, 2164–2166 (2010)
8. K.T. Gahagan, G.A. Swartzlander, Trapping of low-index microparticles in an optical vortex. J. Opt. Soc. Am. **B 15**, 524–534 (1998)
9. J. Arlt, M.J. Padgett, Generation of a beam with a dark focus surrounded by regions of higher intensity: the optical bottle beam. Opt. Lett. **25**, 191–193 (2000)
10. V.G. Shvedov, Y.V. Izdebskaya, A.V. Rode, A. Desyatnikov, W. Krolikowski, Y.S. Kivshar, Generation of optical bottle beams by incoherent white-light vortices. Opt. Express **16**, 20902–20907 (2008)
11. I. Chremmos, P. Zhang, J. Prakash, N.K. Efremidis, D.N. Christodoulides, Z. Chen, Fourier-space generation of abruptly autofocusing beams and optical bottle beams. Opt. Lett. **36**, 3675–3677 (2011)
12. P. Genevet, J. Dellinger, R. Blanchard, A. She, M. Petit, B. Cluzel, M.A. Kats, de F. Fornel, F. Capasso, Generation of two-dimensional plasmonic bottle beams. Opt. Express **21**, 10295–10300 (2013)
13. Y. Kozawa, S. Sato, Optical trapping of micrometer-sized dielectric particles by cylindrical vector beams. Opt. Express **18**, 10828–10833 (2010)
14. L. Huang, H. Guo, J. Li, L. Ling, B. Feng, Z.Y. Li, Optical trapping of gold nanoparticles by cylindrical vector beam. Opt. Lett. **37**, 1694–1696 (2012)
15. M.G. Donato, S. Vasi, R. Sayed, P.H. Jones, F. Bonaccorso, A.C. Ferrari, P.G. Gucciardi, O.M. Maragò, Optical trapping of nanotubes with cylindrical vector beams. Opt. Lett. **37**, 3381–3383 (2012)
16. S.E. Skelton, M. Sergides, R. Saija, M.A. Iatì, O.M. Maragò, P.H. Jones, Trapping volume control in optical tweezers using cylindrical vector beams. Opt. Lett. **38**, 28–30 (2013)
17. V.G. Shvedov, C. Hnatovsky, N. Shostka, W. Krolikowski, Generation of vector bottle beams with a uniaxial crystal. J. Opt. Soc. Am. **B 30**, 1–6 (2013)
18. X.L. Wang, J.P. Ding, W.J. Ni, C.S. Guo, H.T. Wang, Generation of arbitrary vector beams with a spatial light modulator and a common path interferometric arrangement. Opt. Lett. **32**, 3549–3551 (2007)
19. V.V. Kotlyar, A.A. Kovalev, Nonparaxial propagation of a Gaussian optical vortex with initial radial polarization. J. Opt. Soc. Am. **A 27**, 372–380 (2010)
20. B. Gu, Y. Cui, Nonparaxial and paraxial focusing of azimuthal-variant vector beams. Opt. Express **20**, 17684–17694 (2012)
21. A. Niv, G. Biener, V. Kleiner, E. Hasman, Rotating vectorial vortices produced by space-variant subwavelength gratings. Opt. Lett. **30**, 2933–2935 (2005)
22. X.L. Wang, J. Chen, Y.N. Li, J.P. Ding, C.S. Guo, H.T. Wang, Optical orbital angular momentum from the curl of polarization. Phys. Rev. Lett. **105**, 253602 (2010)
23. H. Chen, J. Hao, B.F. Zhang, J. Xu, J.P. Ding, H.T. Wang, Generation of vector beam with space-variant distribution of both polarization and phase. Opt. Lett. **36**, 3179–3181 (2011)
24. S. Liu, P. Li, T. Peng, J.L. Zhao, Generation of arbitrary spatially vaiant polarization beams with a trapezoid Sagnac interferometer. Opt. Express **20**, 21715–21721 (2012)
25. B. Tian, J. Pu, Tight focusing of a double-ring-shaped, azimuthally polarized beam. Opt. Lett. **36**, 2014–2016 (2011)
26. P.T. Tai, W.F. Hsieh, C.H. Chen, Direct generation of optical bottle beams from a tightly focused end-pumped solid-state laser. Opt. Express **12**, 5827–5833 (2004)
27. M. Rashid, O.M. Maragò, P.H. Jones, Focusing of high order cylindrical vector beams. J. Opt. A: Pure Appl. Opt. **11**, 065204 (2009)